Diffraction and Total Cross-Section at the Tevatron and the LHC

M. Deile[1], G. Anelli[1], A. Aurola[2], V. Avati[1], V. Berardi[3], U.Bottigli[4], M. Bozzo[5], E. Brücken[2], A. Buzzo[5], M. Calicchio[3], F. Capurro[5], M.G. Catanesi[3], M.A.Ciocci[4], S. Cuneo[5], C. Da Già[6], E. Dimovasili[1], K. Eggert[1], M. Eräluoto[2], F. Ferro[5], A. Giachero[5], J.P. Guillaud[7], J. Hasi[6], F. Haug[1], J. Heino[2], T. Hilden[2], P. Jarron[1], J. Kalliopuska[2], J. Kašpar[8], J. Kempa[9], C. Kenney[10], A. Kok[6], V. Kundrát[8], K. Kurvinen[2], S. Lami[4], J. Lämsä[2], G. Latino[4], R. Lauhakangas[2], J. Lippmaa[2], M. Lokajíček[8], M. LoVetere[5], D. Macina[1], M. Macrí[5], M. Meucci[4], S. Minutoli[5], A. Morelli[5], P. Musico[5], M. Negri[5], H. Niewiadomski[1], E. Noschis[1], J. Ojala[2], F. Oljemark[2], R. Orava[2], M. Oriunno[1], K. Österberg[2], R.Paoletti[4], S. Parker[11], A.-L. Perrot[1], E. Radermacher[1], E. Radicioni[3], E. Robutti[5], L. Ropelewski[1], G. Ruggiero[1], H. Saarikko[2], G.Sanguinetti[4], A. Santroni[5], S. Saramad[1], F. Sauli[1], A.Scribano[4], G. Sette[5], J. Smotlacha[8], W. Snoeys[1], C. Taylor[12], A. Toppinen[2], N.Turini[4], N. Van Remortel[2], L. Verardo[5], A. Verdier[1], S. Watts[6], and J. Whitmore[13]

[1] CERN, Genève, Switzerland
[2] Helsinki Institute of Physics and University of Helsinki, Finland
[3] INFN Sezione di Bari and Politecnico di Bari, Bari, Italy
[4] Università di Siena and Sezione INFN-Pisa, Italy
[5] Università di Genova and Sezione INFN, Genova, Italy
[6] Brunel University, Uxbridge, UK
[7] LAPP Annecy, France
[8] Academy of Sciences of the Czech Republic and Institute of Physics, Praha, Czech Republic
[9] Warsaw University of Technology, Plock, Poland
[10] Molecular Biology Consortium, SLAC, USA
[11] University of Hawaii, USA
[12] Case Western Reserve University, Dept. of Physics, Cleveland, OH, USA
[13] Penn State University, Dept. of Physics, University Park, PA, USA

Abstract. At the Tevatron, the total $p\bar{p}$ cross-section has been measured by CDF at 546 GeV and 1.8 TeV, and by E710/E811 at 1.8 TeV. The two results at 1.8 TeV disagree by 2.6 standard deviations, introducing big uncertainties into extrapolations to higher energies. At the LHC, the TOTEM collaboration is preparing to resolve the ambiguity by measuring the total pp cross-section with a precision of about 1 %. Like at the Tevatron experiments, the luminosity-independent method based on the Optical Theorem will be used. The Tevatron experiments have also performed a vast range of studies about soft and hard diffractive events, partly with antiproton tagging by Roman Pots, partly with rapidity gap tagging. At the LHC, the combined CMS/TOTEM experiments will carry out their diffractive programme with an unprecedented rapidity coverage and Roman Pot spectrometers on both sides of the interaction point. The physics menu comprises detailed studies of soft diffractive differential cross-sections, diffractive structure functions, rapidity gap survival and exclusive central production by Double Pomeron Exchange.

1 Introduction

Elastic and diffractive scattering (see Fig. 1, left) represent a significant fraction (44 % at both $\sqrt{s} = 1.8$ TeV and 14 TeV) of the total pp or $p\bar{p}$ cross-section. Many details of these processes with close ties to proton structure and low-energy QCD are still not understood. The main signature – large gaps in the scattering products' rapidity distribution due to exchange of colour singlets between the interacting protons – leads to the requirement of a good rapidity coverage up to the very forward region. This is also needed for the detection of high-p_T particles and jets

from hard diffractive events – i.e. those with hard partonic subprocesses – which convey information about the partonic structure of the colour singlet (a.k.a. "Pomeron") exchanged. A big fraction of diffractive events exhibits surviving ("leading") protons at very small scattering angles which can be detected in Roman Pot detectors far away from the interaction point.

Another purpose of high-coverage detector systems is the luminosity-independent determination of the total cross-section based on the Optical Theorem which requires the measurement of the total elastic and inelastic rates and the
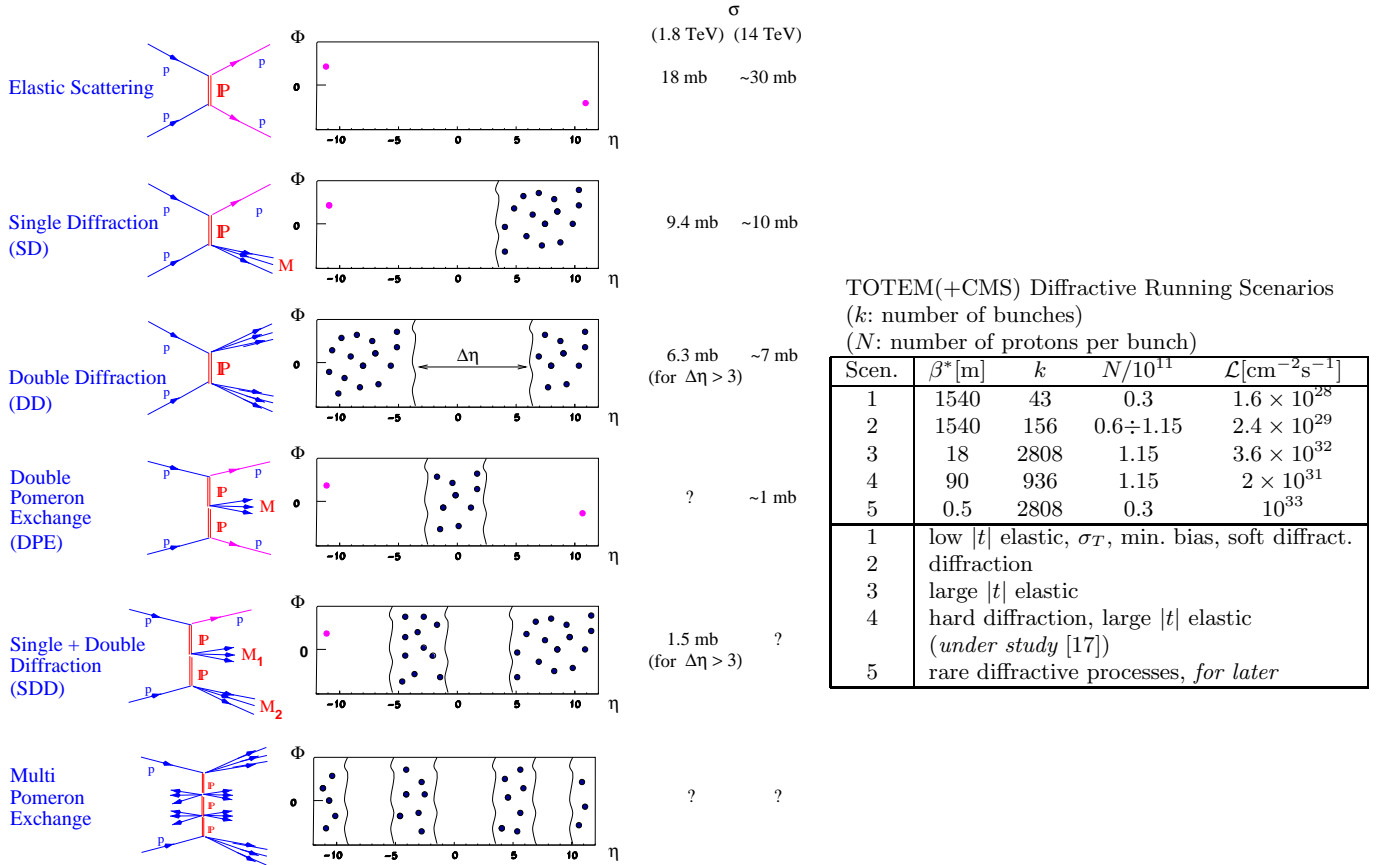
TOTEM(+CMS) Diffractive Running Scenarios
(k: number of bunches)
(N: number of protons per bunch)

Scen.	β^*[m]	k	$N/10^{11}$	$\mathcal{L}[\mathrm{cm}^{-2}\mathrm{s}^{-1}]$
1	1540	43	0.3	1.6×10^{28}
2	1540	156	$0.6 \div 1.15$	2.4×10^{29}
3	18	2808	1.15	3.6×10^{32}
4	90	936	1.15	2×10^{31}
5	0.5	2808	0.3	10^{33}
1	low $|t|$ elastic, σ_T, min. bias, soft diffract.			
2	diffraction			
3	large $|t|$ elastic			
4	hard diffraction, large $|t|$ elastic (*under study* [17])			
5	rare diffractive processes, *for later*			

Fig. 1. Left: diffractive process classes and their cross-sections at Tevatron and LHC. Right: running scenarios for diffractive physics at LHC; for more details see [8].

extrapolation of the nuclear elastic scattering cross-section $d\sigma/dt$ to zero momentum transfer, $t = 0$, as explained in Section 3.

The Tevatron experiments CDF [2], E710 [3] and its very similar successor E811 [4] had Roman Pots on both sides of the interaction points for detecting elastically scattered protons. For diffractive physics, only the antiproton side had enough dispersion for measuring leading particle momenta with Roman Pot spectrometers. The rapidity coverage for measuring the inelastic rate ranged from 5.2 to 6.5 at E710/811 and from 3.2 to 6.7 at CDF. For tagging diffractive events by their rapidity gaps, additional central detectors were available extending the coverage to $\pm(3.8 \div 6.5)$ for E710 and $0 \div (\pm 5.9)$ (7.5) for CDF in Run I (Run II).

At DØ, a double-arm Roman Pot spectrometer (FPD) was installed for Run II [5], allowing to measure elastic and diffractive processes with (anti-) proton acceptance on both sides of the interaction point. In Run I, rapidity gap tagging was possible for $|\eta| < 5.9$.

The TOTEM experiment [1] at the LHC will have Roman Pot stations at 147 m and at 220 m from the interaction point, on both sides. The inelastic event rate will be measured in a rapidity interval from 3.1 to 6.5. For diffractive physics, TOTEM will collaborate with CMS, resulting in a rapidity coverage from 0 to ± 6.5.

2 Elastic pp and p$\bar{\mathrm{p}}$ Scattering

The elastic scattering cross-section $d\sigma/dt$ is characterised by several t-regions with different behaviour (see Fig. 2):

– The Coulomb region where elastic scattering is dominated by photon exchange; this region lies at $|t| < 1.2 \times 10^{-3}$ GeV^2 for $\sqrt{s}$=546 GeV, $|t| < 0.9 \times 10^{-3}$ GeV^2 for $\sqrt{s}$=1.8 TeV, and $|t| < 6.5 \times 10^{-4}$ GeV^2 for $\sqrt{s}$=14 TeV.
– The nuclear/Coulomb interference region, where the cross-section is given by

$$\frac{d\sigma_{el}}{dt} = \pi |f_C e^{-i\alpha\phi(t)} + f_N|^2$$
$$= \pi \left| -\frac{2\alpha G^2(t)}{|t|} e^{-i\alpha\phi(t)} + \frac{\sigma_{tot}}{4\pi} |i + \rho| e^{-B|t|/2} \right|^2 . \quad (1)$$

Here, $G(t)$ is the electromagnetic form factor of the proton, ρ the ratio between real and imaginary part of the forward nuclear elastic amplitude,

$$\rho = \frac{\mathcal{R}[f_{el}(0)]}{\mathcal{I}[f_{el}(0)]} , \quad (2)$$

and ϕ is the relative phase between the nuclear and Coulomb amplitudes. E710 and E811 [3,4] have measured ρ and B in this region (see Table 1), using the
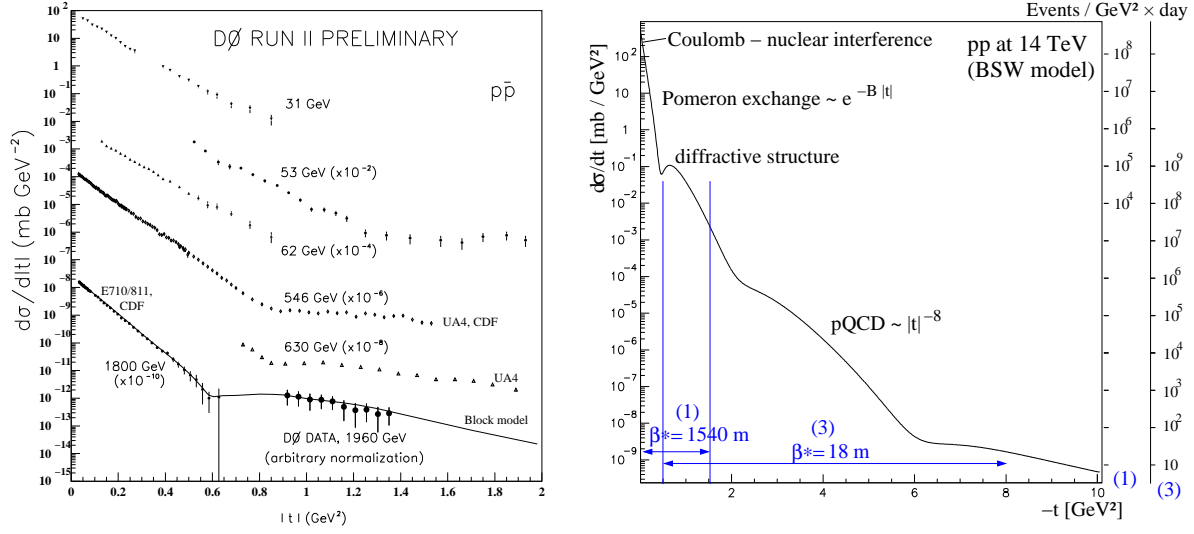
Fig. 2. Left: elastic $p\bar{p}$ scattering from ISR to Tevatron (taken from [7]); right: prediction for elastic pp scattering at LHC; the one-day statistics on the right-hand scales correspond to the running scenarios 1 and 3 (defined in Fig. 1).

West-Yennie parameterisation for $\phi(t)$ [6]. The interest of ρ lies in its predictive power for σ_{tot} at higher energies via the dispersion relation

$$\rho(s) = \frac{\pi}{2\sigma_{tot}(s)} \frac{d\sigma_{tot}}{d\ln s} \qquad (3)$$

- The "single-Pomeron exchange" region with a cross-section $d\sigma/dt \propto \mathrm{e}^{-B\,|t|}$. The parameter B was measured by several Tevatron experiments (Table 1).
- A region with diffractive minima which move to lower $|t|$ as the energy increases (Fig. 2, left).
- The triple-gluon exchange region at high $|t|$ described by perturbative QCD and showing a cross-section proportional to $|t|^{-8}$.

Table 1. Elastic scattering at the Tevatron [3,4,2,7]

$\sqrt{s}$	Exp.	t-range [GeV^2]	B[GeV^{-2}], ρ
546 GeV	CDF	$0.025 \div 0.08$	$B = 15.28 \pm 0.58$
1.8 TeV	CDF	$0.04 \div 0.29$	$B = 16.98 \pm 0.25$
	E710	$0.034 \div 0.65$	$B = 16.3 \pm 0.3$
		$0.001 \div 0.14$	$B = 16.99 \pm 0.25$
			$\rho = 0.140 \pm 0.069$
	E811	$0.002 \div 0.035$	using $\langle B \rangle_{\mathrm{CDF,E710}}$
			$\rho = 0.132 \pm 0.056$
1.96 TeV	DØ	$0.9 \div 1.35$	$-$

The TOTEM experiment at LHC will cover the $|t|$-range from $2 \times 10^{-3}\,\mathrm{GeV}^2$ to $8\,\mathrm{GeV}^2$ (Fig. 2, right) with two running scenarios with special beam optics and different luminosities (scenarios 1 and 3 (or 4) in Fig. 1, right). For details of the t-acceptances of the scenarios see Ref. [8]. The minimum $|t|$-value corresponds to a distance of $1.3\,\mathrm{mm} = 10\,\sigma_{beam} + 0.5\,\mathrm{mm}$ between the Roman Pot at $220\,\mathrm{m}$ and the beam centre. Reaching the Coulomb-nuclear interference region to measure ρ will be attempted

either by approaching the beam closer with the Roman Pot or by operating the LHC at $\sqrt{s} \leq 6\,\mathrm{TeV}$ (see Fig. 4 in [8]).

3 Total pp and p$\bar{\text{p}}$ Cross-Section

The total **pp** or **p$\bar{\text{p}}$** cross-section is related to nuclear elastic forward scattering via the Optical Theorem which can be expressed as

$$\mathcal{L}\sigma_{tot}^2 = \frac{16\pi}{1+\rho^2} \cdot \left. \frac{dN_{el}}{dt} \right|_{t=0} . \qquad (4)$$

With the additional relation

$$\mathcal{L}\sigma_{tot} = N_{el} + N_{inel} \qquad (5)$$

one obtains a system of 2 equations which can be resolved for σ_{tot} or $\mathcal{L}$ independently of each other:

$$\sigma_{tot} = \frac{16\pi}{1+\rho^2} \cdot \frac{dN_{el}/dt|_{t=0}}{N_{el}+N_{inel}} , \qquad (6)$$

$$\mathcal{L} = \frac{1+\rho^2}{16\pi} \cdot \frac{(N_{el}+N_{inel})^2}{dN_{el}/dt|_{t=0}} \qquad (7)$$

Hence the quantities to be measured are:

- the nuclear part of the elastic cross-section extrapolated to $t = 0$;
- the total elastic and inelastic rate, the latter consisting of diffractive (18 mb at LHC) and minimum bias (65 mb at LHC) events.

The ρ parameter has to be taken from external knowledge unless it can be measured from elastic scattering in the interference region between nuclear and Coulomb scattering. CDF have measured σ_{tot} at $546\,\mathrm{GeV}$ and $1.8\,\mathrm{TeV}$
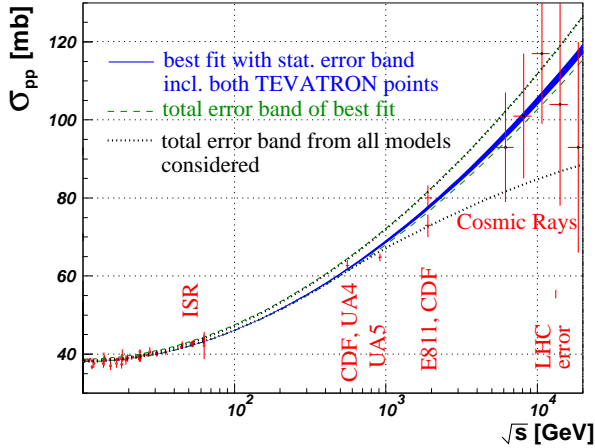
Fig. 3. COMPETE fits [10] to all available pp and $p\bar{p}$ scattering data with statistical (blue solid) and total (green dashed) error bands, the latter taking into account the Tevatron ambiguity. The outermost curves (dotted) give the total error band from all parameterisations considered.

using Eqn. (6) with $\rho = 0.15$ [2] (see Table 2). Their measurement at $546\,\mathrm{GeV}$ agrees with the value from UA4 [9]. E710 and E811 have determined ρ and σ_{tot} simultaneously at $1.8\,\mathrm{TeV}$ [3,4] by combining Eqns. (4) and (5) with (1). Their result for σ_{tot} differs from CDF's number by 2.6 standard deviations. The origin of the discrepancy is unknown.

Table 2. Measurements of the total pp or $p\bar{p}$ cross-section for $\sqrt{s} \geq 546\,\mathrm{GeV}$ and expectations for the LHC.

$\sqrt{s}$	Experiment	σ_{tot} [mb]
546 GeV	UA4	61.9 ± 1.5
	CDF	61.26 ± 0.93
1.8 TeV	CDF	80.03 ± 2.24
	E710	72.8 ± 3.1
	E811	71.42 ± 2.41
14 TeV	(extrapolation [10] to LHC)	$111.5 \pm 1.2^{+4.1}_{-2.1}$
	TOTEM	$? \pm 1$

TOTEM will follow the same method as CDF. The total expected uncertainty of $1\,\%$ after 1 day of taking data at $\mathcal{L} = 1.6 \times 10^{28}\,\mathrm{cm}^{-2}\,\mathrm{s}^{-1}$ will have the following contributions (combined in quadrature):

– The statistical errors of $N_{el} + N_{inel}$ and $dN_{el}/dt|_{t=0}$ are negligible: $0.01\,\%$ and $0.07\,\%$ respectively.
– The systematic error of the total rate stems primarily from trigger losses and amounts to $0.8\,\%$.
– The systematic error of the extrapolation of the elastic cross-section to $t = 0$ is dominated by the theoretical uncertainty of the functional form ($0.5\,\%$). The next-to-leading contributions come from beam energy, alignment and crossing-angle uncertainties (each typically $0.1\,\%$).
– If ρ cannot be measured, the uncertainty in its prediction (e.g. $\rho = 0.1361 \pm 0.0015^{+0.0058}_{-0.0025}$ [10]) will contribute another $0.2\,\%$.

The ATLAS collaboration proposes [11] to extract the four parameters σ_{tot}, ρ, B and $\mathcal{L}$ from a fit to (1) and using $dN/dt = \mathcal{L}d\sigma/dt$. The main difficulties of this approach lie in reaching low enough t-values ($-t < 6 \times 10^{-4}\,\mathrm{GeV}^2$) and in the uncertainty of the phase ϕ.

4 Diffraction

At Tevatron, a vast number of studies on soft and hard diffraction has been carried out (see Table 3 for a brief overview).

Table 3. The diffractive programmes of the Tevatron experiments, the methods for tagging diffractive events, and the coverage in kinematic variables (t is given in units of GeV^2) The abreviations for the diffractive event classes are defined in Fig. 1 (left).

Exp., Run	Tagging	Coverage	Physics
E710 [3]	rap. gap leading $\bar{p}$	$3.8 < |\eta| < 6.5$ $0.05 < -t < 0.11$ $\xi < 0.01$	} soft SD
CDF I,0 [2]	rap. gap leading $\bar{p}$	$|\eta| < 6.7$ $-t < 0.4$ $\xi < 0.2$	} soft SD
CDF IA,B [12]	rap. gap no RP	$|\eta| < 5.9$	soft SD, DD, DPE, SDD
CDF IC [13]	rap. gap leading $\bar{p}$	$|\eta| < 5.9$ $-t < 1$ $0.03 < \xi < 0.1$	hard diffract.: dijets, W, b$\bar{\mathrm{b}}$, J/Ψ
CDF II [14]	rap. gap leading $\bar{p}$	$|\eta| < 7.5$ $-t < 2$ $0.02 < \xi < 0.1$	diffr. struct. funct., search for excl. DPE
DØ I [15]	rap. gap no RP	$|\eta| < 5.9$	hard diffr.: dijets, W, Z
DØ II [7]	rap. gap lead. p, $\bar{p}$	$|\eta| < 5.9$ $0.8 < -t < 2$ any ξ	all above with p, $\bar{p}$ tagging

In Run I, diffractive events were tagged by their rapidity gaps and – in some cases – by a leading antiproton. Leading diffractive protons were not detected. For the ongoing Run II on the other hand, DØ has installed a double-arm proton- and antiproton spectrometer.

At TOTEM/CMS, for all diffractive processes (except DD) leading proton tagging is foreseen with the possibility of using rapidity gaps for redundancy. With scenarios 1 and 2, used for soft and semi-hard diffraction, protons of all ξ will be detected; the total acceptance integrated over t and ξ is $95\,\%$; the resolution in ξ is about 5×10^{-3}. Hard diffraction with its much smaller cross-sections (e.g. $1\,\mu\mathrm{b}$ for SD dijets at $\sqrt{s} = 14\,\mathrm{TeV}$) will be studied with scenario 4 where the total proton acceptance is about $65\,\%$, and the ξ resolution is about 4×10^{-4}.

4.1 Soft Diffraction

At Tevatron, the total and differential soft diffractive cross-sections have been measured for the processes of SD (E710,

CDF), DD and SDD (CDF), see Fig. 1. A central result of these cross-section studies is that the t and ξ dependences of the differential cross-sections conform to the predictions of Regge Theory, but that the total normalisations measured are suppressed, as also observed in hard diffraction (see below). With increasing $\sqrt{s}$ this suppression becomes more pronounced. The behaviour of the diffractive cross-sections at energies above 1.8 TeV is controversial between different models predicting it either to increase further or to remain constant [16]. From the ratios between σ_{diff}, σ_{elast} and σ_{tot}, information about opacity and size of the proton can be deduced.

In DPE, CDF's one-armed antiproton spectrometer tagged the slightly wider "inclusive" event class $\bar{p}p \rightarrow \bar{p} + X + Y$ where the proton is allowed to dissociate into a low-mass system Y with $m_Y^2 \leq 8\,\text{GeV}^2$. In the central diffractive system, masses up to a few 10^2 GeV were seen. At LHC, diffractive masses up to about 1.4 TeV will be observable with sufficient statistics. Surviving protons will be detected on both sides of the IP.

4.2 Hard Diffraction

A central result in diffraction at Tevatron is the breaking of QCD factorisation, i.e. of the hypothesis that the cross-sections of hard diffractive processes can be written as a convolution

$$\sigma = \int d\beta\, dQ^2\, d\xi\, dt\; \hat{\sigma}(\beta, Q^2, \xi, t)\, F_2^D(\beta, Q^2, \xi, t) \quad (8)$$

of a parton-level cross-section $\hat{\sigma}$ and a process-independent diffractive structure function F_2^D. Comparing F_2^D from dijet production in diffractive deep inelastic scattering (DDIS) at HERA with the result from single diffractive dijet production at Tevatron yields a suppression of the latter by roughly a factor 10 (Fig. 4).
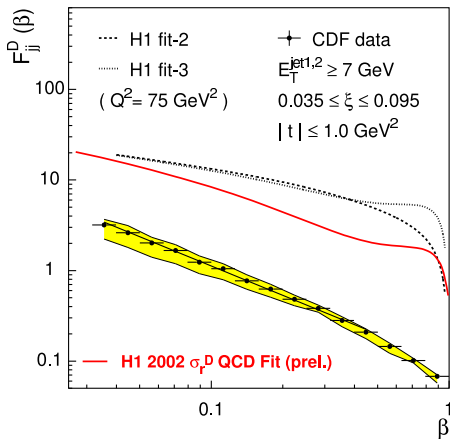

Fig. 4. Diffractive structure function for dijet production in DDIS at H1 and in SD at CDF. The mean $(E_T^{jet})^2$ at CDF corresponds approximately to Q^2 at H1.

This suppression of the diffractive cross-section is independent of the hard subprocess, as can be seen by com-

paring for different partonic subprocesses the fractions of events showing rapidity gaps (Table 4). They are all of the order 1 %. The variations are due to different sensitivities to the gluon and quark components of the Pomeron and led to the determination of the gluon fraction $f_g = 0.59 \pm 0.14 \pm 0.06$ in agreement with HERA's $f_g = 0.75 \pm 0.15$.

Table 4. Ratio R between the diffractive subsample (with rapidity gap) and all events for a given hard subprocess (j = jet, G = gap). $\sqrt{s} = 1.8\,\text{TeV}$.

Process	Cuts	R [%]	Exp.
SD: j + j + G	$E_T > 20\,\text{GeV}$, $\eta_j > 1.8$	0.75 ± 0.10	CDF
	$E_T > 12\,\text{GeV}$, $|\eta_j| > 1.6$	0.65 ± 0.04	DØ
DD: j + G + j	$E_T > 20\,\text{GeV}$, $|\eta_j| > 1.8$	1.13 ± 0.16	CDF
	$E_T > 30\,\text{GeV}$, $|\eta_j| > 1.6$, $\Delta\eta_j > 4$	0.94 ± 0.13	DØ
SD: W + G $\rightarrow e\nu + G$	$\not{E}_T, E_{Te} > 20\,\text{GeV}$	1.15 ± 0.55	CDF
	$\not{E}_T, E_{Te} > 25\,\text{GeV}$	$0.89^{+0.20}_{-0.19}$	DØ
SD: Z + G $\rightarrow ee + G$	$E_{Te} > 25\,\text{GeV}$	$1.44^{+0.62}_{-0.54}$	DØ
SD: b + G $\rightarrow eX + G$	$p_{Te} > 9.5\,\text{GeV}$, $|\eta_e| < 1.1$	0.62 ± 0.25	CDF
SD: J/Ψ + G $\rightarrow \mu^+\mu^- + G$	$p_{T\mu} > 2\,\text{GeV}$, $|\eta_\mu| < 0.6$	1.45 ± 0.25	CDF

A possible explanation lies in the different initial states in DDIS and in proton-antiproton diffraction. In the latter case, additional soft scattering between the two initial hadrons can fill the rapidity gap and thus destroy the signature used for identifying diffractive events. Hence the cross-section in Eqn. (8) needs the "gap survival probability" $|S|^2$ as another convolution factor. $|S|^2$ was observed by CDF to decrease by a factor $1.3 \div 2.4$ from 630 GeV to 1.8 TeV and is expected to be further reduced at LHC energies. The measurement of gap probabilities at the LHC will be an important input for the study of exclusive production processes discussed in the next section.

At LHC, additional hard phenomena offering insight into proton structure are being explored, like exclusive SD into three jets, pp $\rightarrow$ p + jjj, which would indicate a *minimal Fock space* parton configuration $|qqq\rangle$ in the proton [18]. For a jet threshold of 10 GeV, a cross-section between 0.04 and 0.4 nb is predicted, yielding 80 to 800 events per day at $\mathcal{L} = 2 \times 10^{31}\,\text{cm}^{-2}\text{s}^{-1}$ (scenario 4).

4.3 Exclusive Production by DPE

A particularly interesting subclass of DPE events is exclusive central production, characterised by only one single particle or a dijet in the diffractive system. The vacuum quantum numbers of the two colliding colour singlets lead to selection rules on spin J, parity P and charge conjugation C [19]:

$$J^P = 0^+, 2^+, 4^+; J_z = 0; C = +1 \quad (9)$$

(in the limit of $t = 0$). The $J_z = 0$ rule strongly suppresses gg→ q$\bar{q}$ background because of helicity conservation (this background would totally vanish for massless quarks). The rules can also be used for determining the quantum numbers of a new state observed. Table 5 lists some examples for exclusive production. For exclusive dijet and χ_{c0} production, CDF has seen event candidates and set upper limits on the cross-section. At LHC, these processes should be well within reach using scenario 4. The observability of the χ_{b0} is doubtful because the branching ratio for its muonic decay is unknown (upper limit: 10^{-3}).

Table 5. Examples of exclusive DPE processes (p + p → p + X + p). For cross-sections see e.g. [20]. The numbers in square brackets are experimental upper limits from CDF, Run II [14].

Diffractive system	Decay channel	$\sigma(Tev.) \times$BR	$\sigma(LHC) \times$BR
dijet ($E_T > 10$ GeV)	jj	0.97 nb [≤1.1 nb]	7 nb
χ_{c0} (3.4 GeV)	$\gamma J/\psi \to \gamma\mu^+\mu^-$	390 pb [≤204 pb][1]	1.8 nb
	$\pi^+\pi^- K^+K^-$	12 nb	54 nb
χ_{b0} (9.9 GeV)	$\gamma Y \to \gamma\mu^+\mu^-$	≤ 0.5 pb	≤4 pb

[1] scaled from CDF's rapidity range ± 0.6 to ± 2.5 used by KMRS [20].

Table 6. Cross-sections for exclusive Higgs production in the SM and the MSSM (examples) [21]. A mass resolution $\sigma(M) = 3$ GeV from the Roman Pot spectrometer is assumed.

SM, $m_H = 120$ GeV	
$\sigma \times$ BR(H → b$\bar{b}$)	2 fb (S/B @ 30 fb^{-1} = 11/10)
$\sigma \times$ BR(H → WW*)	0.4 fb (S/B @ 30 fb^{-1} = 8/3)

MSSM, $m_A = 130$ GeV	$\tan\beta = \mathbf{30}$ $m_h = 122.7$ GeV $m_H = 134.2$ GeV	$\tan\beta = \mathbf{50}$ $m_h = 124.4$ GeV $m_H = 133.5$ GeV
$\sigma \times$ BR(A → b$\bar{b}$)	0.07 fb	0.2 fb
$\sigma \times$ BR(h → b$\bar{b}$)	5.6 fb	13 fb
$\sigma \times$ BR(H → b$\bar{b}$)	8.7 fb	23 fb
MSSM, $m_A = 100$ GeV	$\tan\beta = \mathbf{30}$ $m_h = 98$ GeV $m_H = 133$ GeV	$\tan\beta = \mathbf{50}$ $m_h = 99$ GeV $m_H = 131$ GeV
$\sigma \times$ BR(A → b$\bar{b}$)	0.4 fb	1.1 fb
$\sigma \times$ BR(h → b$\bar{b}$)	70 fb	200 fb
$\sigma \times$ BR(H → b$\bar{b}$)	8 fb	15 fb

At a later stage it might even be possible for TOTEM +CMS to observe exclusive production of the Higgs boson. However, the low cross-section requires running at $\mathcal{L} \sim 10^{33}$ cm^{-2}s^{-1}, i.e. with scenario 5 whose optics are such that additional Roman Pots in the cryogenic LHC region at 420 m from the IP would be needed for sufficient leading proton acceptance. Still, the diffractive production rate of a Standard Model Higgs is very low, as is the signal-to-background ratio for the dominant decay channel H → b$\bar{b}$ (see Table 6, top block). More favourable is the MSSM case, particularly for large $\tan\beta$ and low m_A (Table 6, middle and bottom blocks). Due to the selection rules (9), exclusive production of the CP-odd A is suppressed, giving the opportunity to separate it from the CP-even h and H, which is difficult for conventional inclusive production,

particularly in the region of $m_A \approx 130$ GeV where all three neutral Higgs bosons have very similar masses.

References

1. TOTEM: Technical Design Report, CERN-LHCC-2004-002; addendum CERN-LHCC-2004-020.
2. CDF Collaboration (F. Abe et al.), Phys. Rev. **D 50**, (1994) 5518; Phys. Rev. **D 50**, (1994) 5535; Phys. Rev. **D 50**, (1994) 5550;
3. E710 Collaboration (N.A. Amos et al.), PRL **61**, (1988) 525; PRL **63**, (1989) 2784; Phys. Lett. **B 243**, (1990) 158; Phys. Lett. **B 247**, (1990) 127; PRL **68**, (1992) 2433; Phys. Lett. **B 301**, (1993) 313.
4. E811 Collaboration (C. Avila et al.), Phys. Lett. **B 445**, (1999) 419; Phys. Lett. **B 537**, (2002) 41.
5. D0 Collaboration (A. Brandt et al.), A Forward Proton Detector at D0, FERMILAB-PUB-97-377, 1997.
6. G.B. West and D.R. Yennie, Phys. Rev.**172**, (1968) 1413.
7. T. Edwards et al., Elastic and Diffractive Scattering at D0, Proc. of the XII International Workshop on Deep Inelastic Scattering, IEP SAS Košice 2004, pp. 466-471.
8. M. Deile et al., The First Year at LHC: Diffractive Physics; hep-ex/0503042; submitted to Czech.J.Phys.
9. UA4 Collaboration (M. Bozzo et al.), Phys. Lett. **147B** (1984) 392.
10. J.R. Cudell et al.; Benchmarks for the Forward Observables at RHIC, the Tevatron-Run II, and the LHC; PRL **89**, (2002) 201801.
11. ATLAS Forward Detectors for Luminosity Measurement and Monitoring, Letter of Intent, CERN/LHCC/2004-010.
12. CDF Collaboration (F. Abe et al.), PRL **74**, (1995) 855; PRL **78**, (1997) 2698; PRL **79**, (1997) 2636; PRL **80**, (1998) 1156; PRL **81**, (1998) 5278; (T. Affolder et al.), PRL **84**, (2000) 232; PRL **87**, (2001) 241802;
13. CDF Collaboration (T. Affolder et al.), PRL **84**, (2000) 5043; PRL **85**, (2000) 4215; PRL **87**, (2001) 141802; PRL **88**, (2002) 151802; PRL **91**, (2003) 011802; PRL **93**, (2004) 141601.
14. For Run II see e.g. K. Terashi on behalf of the CDF Collaboration, Diffractive Measurements at CDF, Proc. of the XII International Workshop on Deep Inelastic Scattering, IEP SAS Košice 2004, pp. 546-553.
15. D0 Collaboration (S. Abachi et al.), PRL **72**, (1994) 2332; PRL **76**, (1996) 734; Phys. Lett. **B 440**, (1998) 189; Phys. Lett. **B 531**, (2002) 52; Phys. Lett. **B 574**, (2003) 169;
16. K. Goulianos, Phys. Lett. **B 358**, (1995) 379; S. Sapeta and K. Golec-Biernat, Phys. Lett. **B 613**, (2005) 154.
17. K. Eggert et al., TOTEM physics, proceedings from the XIth International Conference on Elastic and Diffractive Scattering, Blois 2005.
18. L. Frankfurt, M. Strikman, Surveys High Energ.Phys. **14** (1999) 9-27; A. Ageev et al. (FELIX Collaboration), J. Phys. G **28**, (2002) R117.
19. V.A. Khoze, A.D. Martin, M.G. Ryskin, Eur. Phys. J. C19 (2001) 477.
20. V.A. Khoze et al., Eur. Phys. J. **C23** (2002) 311.; Eur. Phys. J. C35 (2004) 211-220. V.A. Petrov, R.A. Ryutin, JHEP 0408 (2004) 013.
21. A.B. Kaidalov et al., Eur. Phys. J. **C33**, (2004) 261.